The maximal axial parameters in equivalent parametrizations of crystal-field Hamiltonians of tetragonal and cubic symmetries

J. Mulak[1], M. Mulak[2] and R. Gonczarek[2]

[1] *Trzebiatowski Institute of Low Temperature and Structure Research,*
Polish Academy of Sciences, 50–950, PO Box 1410, Wroclaw, Poland
[2] *Institute of Physics, Wroclaw University of Technology,*
Wyb. Wyspianskiego 27, 50–370 Wroclaw, Poland

Abstract

The variation ranges of the axial B_{k0} crystal-field parameters, for $k = 2, 4, 6$, of tetragonal including cubic crystal-field Hamiltonians $\mathcal{H}_{CF}$ for all possible orientations of the relevant reference frame are studied. The distinguished z-axis directions fixed by the maximal absolute values of B_{k0} are analyzed. The diagrams for any tetragonal $\mathcal{H}_{CF}$ parametrization depicting the maximal values of $\frac{|B_{k0}|}{M_k}$, where M_k is the 2^k-pole modulus, as a function of the $x = \frac{B_{k4}}{B_{k0}}$ or $\frac{B_{64}}{B_{60}}$ ratios, together with the distinguished directions are presented. The $\frac{max|B_{k0}|}{M_k}$ magnitudes and the relevant distinguished directions are the discriminants of all the equivalent parametrizations. They vary within the intervals $(0.7395, 1]$, $(0.6074, 1]$ for tetragonal $k = 4$ and tetragonal $k = 6$ $\mathcal{H}_{CF}$ components, respectively. Such specified directions determine the mutual spatial orientation of the component 2^k-poles of the $\mathcal{H}_{CF}$, and due to their rigid coupling in the $\mathcal{H}_{CF}$, they also refer to the global $\mathcal{H}_{CF}$ parametrization. This approach demonstrates the difference in fitting capability between the real and complex isomodular $\mathcal{H}_{CF}$ parametrizations.

1. Introduction

In the paper by the equivalent $\mathcal{H}_{\mathrm{CF}}$ parametrizations we understand those referring to the same real crystal-field (CF) potential but expressed in variously orientated reference frames. Therefore, they can be reduced to the identical form through the appropriate rotations of the involved reference systems. However, the problem which generally remains, especially in the lower symmetry cases, is the lack of knowledge of the initial reference frame orientation in which the parametrization has been defined. The equivalent parametrizations can be identified and distinguished by their maximal axial parameters B_{k0} or their maximal absolute values, $\max|B_{k0}|$, achieved in the specified reference frames. In general,

$$\max|B_{k0}| \leq M_k = \left\{ \sum_q |B_{kq}|^2 \right\}^{1/2} \qquad \text{reach the } M_k \text{ values only under certain conditions for the crystal-}$$

field parameters (CFPs) ratios. It has been shown that the $\max \frac{|B_{k0}|}{M_k}$ magnitudes turn out to be useful discriminants of the equivalent parametrizations [1]. In the case of CF potentials of tetragonal and cubic symmetries expressed in their symmetry-adapted reference frames, there is no difficulty to establish such an initial frame orientation taking the four-fold axis as the z-axis. The only ambiguity resulting from the double choice of the x and y axes directions manifests itself solely in the change of sign of the tetragonal $B_{k\pm4}$ CFPs [2]. The absolute values of the $|x_{44}| = |\frac{B_{44}}{B_{40}}|$ and $|x_{64}| = |\frac{B_{64}}{B_{60}}|$ ratios appear to be sufficient for the complete and explicit description of the parameterizations.

There are in sum twelve point symmetry groups of the tetragonal and cubic symmetries. The parametrizations of the corresponding $\mathcal{H}_{\mathrm{CF}}$s split into two kinds [3,4,5]. The first concerns the tetragonal I [6] (D_4, C_{4v}, D_{2d}, D_{4h}) and the cubic (T, T_h, O, T_d, O_h) point symmetries with purely real CFPs: 5 and 2, respectively. The second concerns the tetragonal II [6] (C_4, S_4, C_{4h}) point symmetries which need nominally 7 CFPs, including the two pairs of complex ones.

In compliance with the tetragonal point symmetry of the central ion its $\mathcal{H}_{\mathrm{CF}}$ parametrizations can include at most one pair of complex-conjugate CFPs per component multipole (except the quadrupole): B_{44}, B_{4-4}; B_{64}, B_{6-4}. It means that the component multipoles parametrizations treated separately can always be reduced to a real three-parameter form. This reduction can be achieved by the appropriate reference system rotation about its z-axis [7].

Since the individual multipoles are characterized by the separate irreducible representations of the three-dimensional rotation group, the maximal B_{k0} variation ranges and the relevant distinguished directions are analyzed for each multipole individually. So, we use the real form of the $\mathcal{H}_{\mathrm{CF}}$ parametrizations as the initial one. The more general complex parametrizations mentioned above are automatically included in the analytical approach based on continuous rotations of the reference frame. Formulating the global $\mathcal{H}_{\mathrm{CF}}$ an additional problem can arise when all the three effective multipoles have to be expressed simultaneously in a common reference frame (either known or a nominal one [8]). Then a pair of B_{k4}, B_{k-4} CFPs ($k = 4$ or 6) can occur in the tetragonal $\mathcal{H}_{\mathrm{CF}}$ parametrizations and an additional degree of freedom (the phase of the complex B_{k4} CFP) is introduced into the fitting procedure. This problem is discussed in subsection 3.4 based on a classical example of S_4 symmetry.

Rotating the initial reference frame by the $(\alpha, \beta, 0)$ Euler angles within the ranges that cover the complete variation of the axial CFPs, two-dimensional functions $B_{k0}(\alpha, \beta)$ are obtained. These graphs or their projections (contour maps) are characterized by the unique arrays of certain points further called the particular points, at which both the partial derivatives $\partial B_{k0}/\partial \beta$ and $\partial B_{k0}/\partial \alpha$ simultaneously equal zero [1]. These particular points can be classified as maxima, minima or saddle points by means of the higher derivatives either directly from the contour-line maps or from the three-dimensional $B_{k0}(\alpha, \beta)$ graphs. It is recommended to present the maps in the normalized and dimensionless form dividing all their values by M_k. According to the orientation of the parametrized CF potential with respect to the initial reference frame, the particular points arrange themselves into

the characteristic constellations. The $\frac{B_{k0}}{M_k}$ values at these points can be degenerate. The maximum values, $\frac{\max|B_{k0}|}{M_k}$, are achieved in one or in several particular points. The plotted functions $\frac{\max|B_{40}|}{M_4}$ (x_{44}), $\frac{\max|B_{60}|}{M_6}$ (x_{64}) allow one to find directly the maximal values and the corresponding distinguished directions for any x ratios. Additionally, these practical schemes give also the values and directions for all the remaining particular points on the maps. It is worth emphasizing that the diagrams have a general character and make allowance for the explicit analysis of any tetragonal $\mathcal{H}_{\mathrm{CF}}$ parametrization. Since the diagrams are of general character all the relevant dimensionless values are given with a fairly high accuracy of order of 10^{-4}.

2. General formulation

Throughout the paper the tensor notation (by Wybourne [9]) for the $\mathcal{H}_{\mathrm{CF}}$ parametrizations is consistently used. And so, in the case of the tetragonal I symmetries the parametrization has the form:

$$\mathcal{H}_{\mathrm{CF}}(\text{tetra I}) \quad = \quad B_{20}C_0^{(2)} + B_{40}C_0^{(4)} + B_{44}\left(C_4^{(4)} + C_{-4}^{(4)}\right) + B_{60}C_0^{(6)} + B_{64}\left(C_4^{(6)} + C_{-4}^{(6)}\right), \quad (1)$$

whereas in the case of the tetragonal II symmetries the $B_{k\pm4}$ are complex. In short, $C_q^k = \sum_i C_q^k(\theta_i, \varphi_i)$ where $C_q^k(\theta_i, \varphi_i)$ are the normalized spherical harmonics [4,5,9] and the summation runs over i denoting all the open-shell central-ion electrons of the polar coordinates (θ_i, φ_i).

Here we investigate the B_{k0} variation with the z-axis direction defined in an arbitrary reference frame by only two Euler angles $(\alpha, \beta, 0)$ with respect to the initial frame [10,11], where the third angle γ of the rotation about the final z-axis may be assumed to be zero as an arbitrary in the case. The transformed B'_{k0} are related to the original B_{k0} as [1,5,10,11]

$$B'_{k0} = \sum_{q=-k}^{k} \mathcal{D}_{0q}^{(k)}(\alpha, \beta, 0)B_{kq} = \sum_{q=-k}^{k} C_q^{(k)}(\beta, \alpha)B_{kq}, \quad (2)$$

where $\mathcal{D}_{0q}^{(k)}(\alpha, \beta, 0) = C_q^{(k)}(\beta, \alpha)$ are the middle row matrix elements of the $\mathcal{D}^{(k)}(\alpha, \beta, 0)$ rotation matrices [10,11]. Below in the paper B_{kq} correspond to the original reference frame, whereas their primed counterparts B'_{kq} stand for the rotationally transformed ones.

Naturally, all the equivalent $\mathcal{H}_{\mathrm{CF}}$ parametrizations have to be characterized by the same variation ranges of their CFPs including the axial ones, in other words by the ranges with the same upper and lower limits. These particular maximal and minimal values can serve as useful discriminants for the whole classes of the equivalent parametrizations. In order to standardize the equivalent parametrizations the $\frac{\max|B'_{k0}|}{M_k}$ magnitudes can be recommended as the best discriminants. Consequently, the direction of the transformed reference frame z-axis relevant to these discriminants are now the common distinguished directions for all the equivalent parametrizations. This approach is especially useful in the case of low-symmetry CF potentials [1].

The axial CFPs play an extraordinary role since they are real and invariant relative to rotations about the z-axis. They are also independent of the z-axis inversion, whereas the remaining CFPs become then inevitably transformed according to the rule $B_{kq} \rightarrow B_{k-q}$, as the effect of the rotation by $(0, \pi, 0)$.

The relationship between B'_{k0} CFPs and the two rotation angles $(\alpha, \beta, 0)$ of the reference frame can be expressed in the form of two-dimensional contour maps $\frac{B'_{k0}(\alpha, \beta)}{M_k}$ with iso-$\frac{B'_{k0}}{M_k}$ lines joining the points of identical $\frac{B'_{k0}}{M_k}$ values. For the equivalent parametrizations such maps can be always transformed into each other. The whole ranges of the rotation angles variation $0 \leq \alpha \leq 2\pi$ and $0 \leq \beta \leq \pi$ can be

limited according to the $\mathcal{H}_{\mathrm{CF}}$ symmetry. For the tetragonal symmetries (I and II) with the z-axis along the four-fold axis the maps are periodical functions of α with the period of $\pi/2$. Furthermore, since B'_{k0} CFPs are the same at points (α, β) and $(\alpha+\pi, \pi-\beta)$, what results from their independence of the z-axis orientation, the range of β can be confined to the interval $(0, \pi/2)$. For the clarity reasons the maps are presented within the ranges $0 \leq \alpha \leq \pi$ and $0 \leq \beta \leq \pi$.

As the paper concerns exclusively the rotational transformations of the axial B_{k0} CFPs, only the middle rows of the relevant rotation matrices $\mathcal{D}^{(k)}(\alpha, \beta, 0)$ [10,11] are employed. All the non-axial CFPs transform themselves according to the remaining rows [5,10,11]. After the initial reference frame rotation the $\mathcal{H}_{\mathrm{CF}}$ form obeys the central-ion point symmetry with respect to the new frame. Additionally, in the distinguished reference frames some correlations between the CFPs can occur, like that found by Burdick and Reid [12]. They proved analytically that the $B_{k\pm1}$ CFPs become zero at the maximum, minimum and saddle points of the $B_{k0}(\alpha, \beta)$ functions.

3. The axial components in equivalent parametrizations of tetragonal and cubic $\mathcal{H}_{\mathrm{CF}}$s as functions of $\frac{B_{44}}{B_{40}}$ or $\frac{B_{64}}{B_{60}}$ ratios

3.1 The 2^2-pole axial parameter B_{20} in arbitrarily oriented reference frame

In cubic potentials the quadrupolar moment is completely compensated and, in consequence, its components do not appear in any reference frame. Hence, in the most general case the cubic $\mathcal{H}_{\mathrm{CF}}$ can be parametrized by at most 22 instead of 27 CFPs.

For the tetragonal potential expressed in the symmetry-adapted system there exists only the axial term $B_{20}C_0^{(2)}$. In any other reference frame rotated by α and β one gets [1,10,11]:

$$B'_{2q} = B_{20}\mathcal{D}_{q0}^{(2)}(\alpha, \beta, 0) = (-1)^q C_q^{(2)}(\beta, \alpha)B_{20}, \tag{3}$$

and the ratios $\frac{B'_{2q}}{B_{20}}$ for different q are correlated. For $q = 0$

$$B'_{20} = \frac{1}{2}\left(3c^2 - 1\right)B_{20}, \tag{4}$$

where $c = \cos\beta$ and thus B'_{20} depends solely on β. The derivative $\partial B'_{20}/\partial\beta = -3csB_{20}$, where $s = \sin\beta$, and is equal to zero for $\beta = 0, \pi$ or $\pi/2$. For these β values B'_{20} reaches its extreme magnitudes: B_{20} and $-\frac{1}{2}B_{20}$, respectively. Hence, the distinguished direction for which $\frac{|B'_{20}|}{M_2}$ achieves 1 is the symmetry axis, whereas in the symmetry adapted system $\frac{B_{20}}{M_2}$ equals 1 automatically. For $\beta = \arccos\frac{1}{\sqrt{3}}$, which is the angle between the edge and diagonal in a cube, B'_{20} vanishes, but then the four remaining CFPs appear: $|B'_{22}| = |B'_{2-2}| = \frac{\sqrt{6}}{6}B_{20}$ and $|B'_{21}| = |B'_{2-1}| = \frac{\sqrt{3}}{3}B_{20}$.

3.2 The 2^4-pole axial parameter B_{40} in arbitrarily oriented reference frame

The fourth-order $\mathcal{H}_{\mathrm{CF}}$ term in the tetragonal I and cubic CF potentials described in the symmetry-adapted system has the form [3-5,13]

$$\mathcal{H}_{\mathrm{CF}}^{(IV)} = B_{40}\left[C_0^{(4)} + x_4\left(C_4^{(4)} + C_{-4}^{(4)}\right)\right], \tag{5}$$

and the modulus of the 2^4-pole is equal to

$$M_4 = |B_{40}|(1 + 2x_4^2)^{1/2}. \tag{6}$$

For the cubic case $x_4 = \sqrt{\frac{5}{14}} = 0.5976$ [6,7,13]. Eq.(3) yields for any rotation by α and β the relation:

$$B'_{40} = \frac{1}{8}\left[3 - 30c^2 + 35c^4 + x_4\sqrt{70}s^4\cos 4\alpha\right]B_{40}. \tag{7}$$

Therefore,

$$\frac{B'_{40}}{M_4} = \frac{3 - 30c^2 + 35c^4 + x_4\sqrt{70}s^4\cos 4\alpha}{8(1 + 2x_4^2)^{1/2}} \cdot \frac{B_{40}}{|B_{40}|}. \tag{8}$$

Using Eq.(9) for any x_4 the map $\frac{B'_{40}}{M_4}(\alpha, \beta)$ can be depicted within the required ranges of α and β angles. The partial derivatives

$$\frac{1}{M_4}\frac{\partial B'_{40}}{\partial \beta} = \frac{cs(15 - 35c^2 + x_4\sqrt{70}s^2\cos 4\alpha)}{2(1 + 2x_4^2)^{1/2}} \cdot \frac{B_{40}}{|B_{40}|}$$

$$\frac{1}{M_4}\frac{\partial B'_{40}}{\partial \alpha} = -\frac{x_4\sqrt{70}s^4\sin 4\alpha}{2(1 + 2x_4^2)^{1/2}} \cdot \frac{B_{40}}{|B_{40}|} \tag{9}$$

simultaneously vanish in the following five cases:

$$
\begin{aligned}
a) \quad & s = 0, \\
b) \quad & c = 0, \quad \cos 4\alpha = 1, \\
c) \quad & c = 0, \quad \cos 4\alpha = -1, \\
d) \quad & 15 - 35c^2 + x_4\sqrt{70}s^2 = 0, \quad \cos 4\alpha = 1, \\
e) \quad & 15 - 35c^2 + x_4\sqrt{70}s^2 = 0, \quad \cos 4\alpha = -1,
\end{aligned} \tag{10}
$$

which correspond to the following points on the map $\frac{B'_{40}}{M_4}(\alpha, \beta)$

$$
\begin{aligned}
a) \quad & \beta = 0, \\
b) \quad & \beta = \frac{\pi}{2}, \quad \alpha = 2n\frac{\pi}{4}, \\
c) \quad & \beta = \frac{\pi}{2}, \quad \alpha = (2n+1)\frac{\pi}{4}, \\
d) \quad & \beta = \arccos\left(\frac{x_4\sqrt{70} + 15}{x_4\sqrt{70} + 35}\right)^{1/2}, \quad \alpha = 2n\frac{\pi}{4} \\
e) \quad & \beta = \arccos\left(\frac{x_4\sqrt{70} - 15}{x_4\sqrt{70} - 35}\right)^{1/2}, \quad \alpha = (2n+1)\frac{\pi}{4}.
\end{aligned} \tag{11}
$$

In Eqs (11) n stands for any integer. Let us denote by $|B_{40}^{(i)}|$, $i = a \ldots e$, the absolute value of B_{40} for the (i)-th condition in Eq.(10). Since the plots $\frac{|B_{40}^{(i)}|}{M_4}(x_4)$ for (a) and for the pairs (b, c) and (d, e) are symmetrical with respect to x_4 (Eqs 8, 11), only the positive values of x_4 are taken into account.

For each condition (Eqs 10, 11) the expressions $\frac{|B_{40}^{(i)}|}{M_4}(x_4)$ can be represented by the following plots (Eq. 8):

a) $\frac{|B_{40}^{(a)}|}{M_4}(x_4) = (1 + 2x_4^2)^{-1/2}$
   For $x_4 = 0$, i.e. for the purely axial $\mathcal{H}_{CF}$, this function reaches maximum 1. For the cubic case $(x_4 = 0.5976)$ it amounts to 0.7638, and monotonically falls to zero when $x_4 \to \infty$ (Fig. 2).

5

b) $\frac{|B_{40}^{(b)}|}{M_4}(x_4) = \frac{3+x_4\sqrt{70}}{8\left(1+2x_4^2\right)^{1/2}}$

For $x_4 = 0$ this function equals to 0.3750. For the coplanar square ratio ($x_4 = 1.3944$) it reaches its maximum 0.8292, and then asymptotically decreases to 0.7395 when $x_4 \to \infty$.

c) $\frac{|B_{40}^{(c)}|}{M_4}(x_4) = \frac{|3-x_4\sqrt{70}|}{8\left(1+2x_4^2\right)^{1/2}}$

This function for $x_4 = 0$ takes the same value as in (b) since they are symmetrical. When x_4 rises it drops to zero at $x_4 = 0.3586$, and then monotonically increases to 0.7395 for $x_4 \to \infty$.

d) The condition $0 \le c^2 \le 1$, where $c^2 = \frac{x_4\sqrt{70}+15}{x_4\sqrt{70}+35}$, is fulfilled for all $x_4 \ge 0$ because $x_4 \ge -1.7928$ is sufficient. Substituting the above expression for c^2 and $\cos 4\alpha = 1$ into Eq.8 yields

$\frac{|B_{40}^{(d)}|}{M_4}(x_4) = \frac{|x_4\sqrt{70}-15|}{(x_4\sqrt{70}+35)\left(1+2x_4^2\right)^{1/2}}$

For $x_4 = 0$ the function equals 0.4286, it has zero-point at $x_4 = 1.7928$ and then it pursues zero for $x_4 \to \infty$ passing through the weak and flat maximum 0.0489 at $x_4 = 5.1532$.

e) The condition $0 \le c^2 \le 1$, where $c^2 = \frac{x_4\sqrt{70}-15}{x_4\sqrt{70}-35}$, confines its domain of determinancy to $x_4 \le 1.7928$. Within this range

$\frac{|B_{40}^{(e)}|}{M_4}(x_4) = \frac{x_4\sqrt{70}+15}{(|x_4\sqrt{70}-35|)\left(1+2x_4^2\right)^{1/2}}$.

For $x_4 = 0$ this function equals 0.4286, and for the limiting value $x_4 = 1.7928$ it is 0.5504, i.e. the same as in (c) at that point. Within the interval $0 \le x_4 \le 1.7928$ the plot passes through the subtle local maximum of 0.5092 at $x_4 = 0.5977$, and minimum 0.5065 at $x_4 = 0.9701$.

The plots $\frac{|B_{40}^{(i)}|}{M_4}(x_4)$, $i = a, b, c, d$ and e corresponding to the five conditions (Eqs 10, 11) are presented in Fig. 2. The diagram shows the positions and values of all particular points on the $\frac{B'_{40}}{M_4}(\alpha, \beta)$ map for any tetragonal $\mathcal{H}_{CF}$ as a function of x_4 (see Figs 5-7). Any vertical straight line drawn for a given x_4 intersects the diagram branches (from a to e) in three to five points (depending on the x_4) directly determining the distinguished directions and values including the $\frac{\max|B'_{40}|}{M_4}$.

As is seen from the diagram the four-fold axis, i.e. the initial z-axis direction ([001]), is the distinguished one for $|x_4| \le 0.5976$. For all the remaining x_4, i.e. $|x_4| \ge 0.5976$, this distinguished direction lies along the square diagonal [110]. The crossover point corresponds exactly to the cubic x_4 value. The $\frac{\max|B'_{40}|}{M_4}$ value varies within the range from 1.0000 (for $x_4 = 0$) down to 0.7395 for $x_4 \to \infty$, achieving on the way a local minimum 0.7638 for the cubic x_4 value, and a local maximum 0.8292 for the coplanar square x_4 value.

3.3 The 2^6-pole axial parameter B_{60} in arbitrarily oriented reference frame.

In turn, the sixth-order $\mathcal{H}_{CF}$ term in the tetragonal I and cubic CF potentials in the symmetry adapted system has the form [3-5,13]:

$$\mathcal{H}_{CF}^{(VI)} = B_{60} \left[C_0^{(6)} + x_6 \left(C_4^{(6)} + C_{-4}^{(6)} \right) \right], \tag{12}$$

and the modulus of the 2^6-pole is equal to

$$M_6 = |B_{60}|(1 + 2x_6^2)^{1/2}. \tag{13}$$

For the cubic case $x_6 = \sqrt{\frac{7}{2}} = 1.8708$ [6,7,13]. In the reference frame rotated by $(\alpha, \beta, 0)$ the axial CFP B_{60} transforms to (see Eq.3):

$$B'_{60} = \frac{1}{16} \left[-5 + 105c^2 - 315c^4 + 231c^6 + x_6 3\sqrt{14}s^4(-1 + 11c^2) \cos 4\alpha \right] B_{60}. \tag{14}$$

Hence,

$$\frac{B'_{60}}{M_6} = \frac{-5 + 105c^2 - 315c^4 + 231c^6 + x_6 3\sqrt{14}s^4(-1 + 11c^2)\cos 4\alpha}{16(1 + 2x_6^2)^{1/2}} \cdot \frac{B_{60}}{|B_{60}|}. \tag{15}$$

The particular points of the map $\frac{B'_{60}}{M_6}(\alpha, \beta)$, especially the point (or points) corresponding to the $\frac{\max|B'_{60}|}{M_6}$, are those for which both the partial derivatives $\partial B'_{60}/\partial\beta$ and $\partial B'_{60}/\partial\alpha$ simultaneously become zero

$$\frac{1}{M_6}\frac{\partial B'_{60}}{\partial\beta} = \frac{3}{8}sc\frac{-35 + 210c^2 - 231c^4 + x_6\sqrt{14}(-13 + 46c^2 - 33c^4)\cos 4\alpha}{(1 + 2x_6^2)^{1/2}} \cdot \frac{B_{60}}{|B_{60}|}$$

$$\frac{1}{M_6}\frac{\partial B'_{60}}{\partial\alpha} = -\frac{3}{4}\frac{x_6\sqrt{14}s^4(-1 + 11c^2)\sin 4\alpha}{(1 + 2x_6^2)^{1/2}} \cdot \frac{B_{60}}{|B_{60}|}. \tag{16}$$

There are six possibilities of simultaneous vanishing of the partial derivatives

a) $s = 0$,

b) $c = 0$, $\cos 4\alpha = 1$,

c) $c = 0$, $\cos 4\alpha = -1$,

d) $c^2 = \dfrac{1}{11}$, $\cos 4\alpha = -\dfrac{0.5238}{x_6}$,

e) $(231 + 33\sqrt{14}x_6)c^4 - (210 + 46\sqrt{14}x_6)c^2 + (35 + 13\sqrt{14}x_6) = 0$, $\cos 4\alpha = 1$,

f) $(231 - 33\sqrt{14}x_6)c^4 - (210 - 46\sqrt{14}x_6)c^2 + (35 - 13\sqrt{14}x_6) = 0$, $\cos 4\alpha = -1$. $\tag{17}$

The last two conditions, as the functions of x_6 yield the double solutions, i.e. four solutions for $x_6 > 0.7195$ and three ones for $|x_6| \leq 0.7195$, so in sum there are eight or seven particular points on the map apart from their symmetrical images due to the presence of the four-fold axis as well the invariance of the axial CFPs with respect to the z-axis sense.

The conditions specified above in Eq.17 (from a to f) correspond to the following particular points on the map $\frac{B'_{60}}{M_6}(\alpha, \beta)$:

a) $\beta = 0$,

b) $\beta = \dfrac{\pi}{2}$, $\alpha = 2n\dfrac{\pi}{4}$,

c) $\beta = \dfrac{\pi}{2}$, $\alpha = (2n + 1)\dfrac{\pi}{4}$,

d) $\beta = 72.45^o$, $\alpha = \dfrac{1}{4}\arccos\left(\dfrac{-0.5238}{x_6}\right)$,

e) $\beta = \arccos\left[\dfrac{1}{33}\dfrac{15\sqrt{14} + 46x_6 - 2(100x_6^2 + 48\sqrt{14}x_6 + 210)^{1/2}}{\sqrt{14} + 2x_6}\right]^{1/2}$, $\alpha = 2n\dfrac{\pi}{4}$,

e') $\beta = \arccos\left[\dfrac{1}{33}\dfrac{15\sqrt{14} + 46x_6 + 2(100x_6^2 + 48\sqrt{14}x_6 + 210)^{1/2}}{\sqrt{14} + 2x_6}\right]^{1/2}$, $\alpha = 2n\dfrac{\pi}{4}$,

f) $\beta = \arccos\left[\dfrac{1}{33}\dfrac{15\sqrt{14} - 46x_6 - 2(100x_6^2 - 48\sqrt{14}x_6 + 210)^{1/2}}{\sqrt{14} - 2x_6}\right]^{1/2}$, $\alpha = (2n + 1)\dfrac{\pi}{4}$,

f') $\beta = \arccos\left[\dfrac{1}{33}\dfrac{15\sqrt{14} - 46x_6 + 2(100x_6^2 - 48\sqrt{14}x_6 + 210)^{1/2}}{\sqrt{14} - 2x_6}\right]^{1/2}$, $\alpha = (2n + 1)\dfrac{\pi}{4}$. $\tag{18}$

7

In the cases (d), (e) and (f) the definite domains of determinancy of the involved expressions have to be taken into account. In consequence, the x_6 ratio has to fulfil the following conditions: $|x_6| \geq 0.5238$, $x_6 \geq -0.7195$ and $x_6 \leq 0.7195$, for (d), (e) and (f), respectively.

Unlike for the particular points in $(a-c)$ cases their location in $(d-f)$ cases does depend on the x_6 ratio. The (d) case turns to be quite intriguing. The corresponding particular points (Eq.18d) lie along the straight line $\beta = 72.45^o$, and the $\frac{|B_{60}^{(d)}|}{M_6}(x_6)$ function takes along it the constant value $\frac{0.1322}{(1+2x_6^2)^2}$ regardless of the α rotation angle.

In the (e) case the β angle varies from 90° for the limiting value $x_6 = -0.7195$, through 62.04^0 for $x_6 = 0$, and monotonically goes down to 51.12^o for $x_6 \to \infty$. The $\beta(x_6)$ plot for the (f) case is symmetrical to the previous one with respect to x_6. Similarly, the symmetrical plots for the (e'), Eq.(18e') and (f'), Eq.(18f'), cases are characterized by $\beta = 51.12^o$ for $x_6 \to \mp\infty$, $\beta = 33.88^o$ for $x_6 = 0$, and $\beta = 0$ for $x_6 \to \pm\infty$, respectively (Fig.3). Since the plots $\frac{|B_{60}^{(i)}|}{M_6}(x_6)$ for (a), (d) and the pairs (b, c), (e, f) and (e', f') are symmetrical with respect to x_6 (Eqs 15, 18) only the positive values of x_6 ratio are considered.

For the conditions defined above (Eqs 17,18) the expressions $\frac{|B'_{60}|}{M_6}(x_6)$ reduce themselves (Eq.15) to the following plots:

a) $\frac{|B_{60}^{(a)}|}{M_6}(x_6) = (1 + 2x_6^2)^{-1/2}$
   For $x_6 = 0$ the maximal possible value 1 is reached, for the cubic ratio ($x_6 = 1.8708$) it amounts to 0.3536, and then monotonically falls down to zero as $x_6 \to \mp\infty$.

b) $\frac{|B_{60}^{(b)}|}{M_6}(x_6) = \frac{|-5-3\sqrt{14}x_6|}{16(1+2x_6^2)^{1/2}}$
   For $x_6 = 0$ the function is equal to 0.3125, for the coplanar square ratio ($x_6 = 1.1225$) it reaches its maximum 0.5863, and then slowly falls to the limit 0.4961 as $x_6 \to \infty$.

c) $\frac{|B_{60}^{(c)}|}{M_6}(x_6) = \frac{|-5+3\sqrt{14}x_6|}{16(1+2x_6^2)^{1/2}}$
   As above, for $x_6 = 0$ the function equals 0.3125, and when x_6 rises it falls to zero for $x_6 = 0.4454$, then monotonically increases to the asymptotic value 0.4961 if $x_6 \to \infty$.

d) $\frac{|B_{60}^{(d)}|}{M_6}(x_6) = \frac{0.1322}{(1+2x_6^2)^{1/2}}$
   Here, the domain is limited to $|x_6| \geq 0.5238$, (Eq.18). For $x_6 = 0.5238$ the function amounts to 0.1062 and monotonically tends to zero for $x_6 \to \infty$.

e) $\frac{|B_{60}^{(e)}|}{M_6}(x_6) = \frac{|-5+105t_1(x_6)-315t_1^2(x_6)+231t_1^3(x_6)+x_6 3\sqrt{14}(1-t_1(x_6))^2(-1+11t_1(x_6))|}{16(1+2x_6^2)^{1/2}}$,
   where $t_1(x_6) = \frac{1}{33}\frac{15\sqrt{14}+46x_6-2(100x_6^2+48\sqrt{14}x_6+210)^{1/2}}{\sqrt{14}+2x_6}$, and $x_6 \geq -0.7195$.
   For $x_6 = 0$ the function equals 0.3321. For the cubic ratio ($x_6 = 1.8708$) it reaches quite a subtle maximum 0.6285, and then slowly falls to 0.6074 if $x_6 \to \infty$.

e') $\frac{|B_{60}^{(e')}|}{M_6}(x_6) = \frac{|-5+105t_2(x_6)-315t_2^2(x_6)+231t_2^3(x_6)+x_6 3\sqrt{14}(1-t_2(x_6))^2(-1+11t_2(x_6))|}{16(1+2x_6^2)^{1/2}}$,
   where $t_2(x_6) = \frac{1}{33}\frac{15\sqrt{14}+46x_6+2(100x_6^2+48\sqrt{14}x_6+210)^{1/2}}{\sqrt{14}+2x_6}$.
   For $x_6 = 0$ the expression equals 0.4148, it has zero-point at $x_6 = 1.2481$, next slightly rises to the maximum 0.0710 at $x_6 = 3.6498$, and then slowly falls to zero if $x_6 \to \infty$.

f) $\frac{|B_{60}^{(f)}|}{M_6}(x_6) = \frac{|-5+105t'_1(x_6)-315t_1'^2(x_6)+231t_1'^3(x_6)-x_6 3\sqrt{14}(1-t'_1(x_6))^2(-1+11t'_1(x_6))|}{16(1+2x_6^2)^{1/2}}$,
   where $t'_1(x_6) = \frac{1}{33}\frac{15\sqrt{14}-46x_6-2(100x_6^2-48\sqrt{14}x_6+210)^{1/2}}{\sqrt{14}-2x_6}$ and $x_6 \leq 0.7195$.

For $x_6 = 0$ the function equals 0.3321. At the limiting point ($x_6 = 0.7195$) it amounts to 0.1348, and within the interval ($0 \leq x_6 \leq 0.7195$) the plot passes through the minimum 0.1050 at $x_6 = 0.5595$.

f') $\frac{|B_{60}^{(f')}|}{M_6}(x_6) = \frac{|-5+105t_2'^2(x_6)-315t_2'^2(x_6)+231t_2'^3(x_6)-x_63\sqrt{14}(1-t_2'(x_6))^2(-1+11t_2'(x_6))|}{16(1+2x_6^2)^{1/2}}$,

where $t_2'(x_6) = \frac{1}{33}\frac{15\sqrt{14}-46x_6+2(100x_6^2-48\sqrt{14}x_6+210)^{1/2}}{\sqrt{14}-2x_6}$.

For $x_6 = 0$ the function equals 0.4148 and then monotonically rises to 0.6074 as $x_6 \to \infty$.

The $\frac{|B_{60}^{(i)}|}{M_6}(x_6)$ plots, where $i = a, b, \ldots, f'$, for all the eight conditions (Eqs 17,18) are presented in Fig.4. The straight line corresponding to any chosen x_6 ratio intersects the diagram branches in four to eight points depending on the x_6 value (see Figs 5-7). The points of intersection determine the positions of the particular points and the respective values including the $\frac{\max|B_{60}'|}{M_6}(x_6)$ discriminant. The characteristic degeneracy of some particular point values in the diagrams manifesting itself as the intersection points of their different branches (Figs 2,4) reflects some definite symmetry encoded in the x_6 ratio.

As is seen from the diagram (Fig.4) the four-fold axis, i.e. the initial z-axis direction ([001]), is the distinguished direction for $|x_6| \leq 0.9179$. For all the remaining x_6, i.e. $|x_6| \geq 0.9171$, the distinguished directions (roughly [111]) and the corresponding maximal values are determined by the e-th branch of the diagram. In the cross-over point ($x_6 = 0.9179$) this maximal value amounts to 0.6103. For $x_6 > 0.9179$ the distinguished direction forms with the reference frame z-axis the angle β given by Eq.18e. In the crossover point this angle amounts to 56.69^o, for the cubic ratio ($x_6 = 1.8708$) it equals 54.74^o (exactly [111] direction), and then asymptotically pursues the limit 51.12^o as $x_6 \to \infty$.

The $\frac{\max|B_{60}'|}{M_6}(x_6)$ can vary within the range from 1.0000 (for $x_6 = 0$) to 0.6074 (for $x_6 \to \infty$) passing on the way through the local minimum 0.6103 (for $x_6 = 0.9179$) and the maximum 0.6285 (for $x_6 = 1.8708$). It is worth noticing that the distinguished direction crossover takes place for $x_6 = 0.9179$ which is smaller than both the coplanar square ratio 1.1225 and the cubic ratio 1.8708.

3.4 Tetragonal II $\mathcal{H}_{\mathrm{CF}}$ with complex parameters – the maximal axial CFPs in arbitrarily orientated reference frame

The tetragonal II $\mathcal{H}_{\mathrm{CFS}}$ containing two pairs of B_{k4}, B_{k-4} CFPs ($k = 4, 6$) in the symmetry adapted system deserves more careful analysis. If only one pair of the complex CFPs occurs in the $\mathcal{H}_{\mathrm{CF}}$, there always exists the equivalent real parametrization. The complete parametrization of the tetragonal II $\mathcal{H}_{\mathrm{CF}}$ contains seven instead of five CFPs. Taking into account the rotational properties of $\mathcal{H}_{\mathrm{CF}}$ it is recommended to use the pairs of complex-conjugate parameters: $B_{k4} = |B_{k4}|e^{i4\varphi_{k4}}$ and $B_{k-4} = |B_{k4}|e^{-i4\varphi_{k4}}$ rather than the equivalent pairs $\mathrm{Re}B_{k4}$ and $\mathrm{Im}B_{k4}$. Between the former and latter pairs of the CFPs the following relations hold: $B_{k4} = \mathrm{Re}B_{k4} + i\mathrm{Im}B_{k4}$, $B_{k-4} = \mathrm{Re}B_{k4} - i\mathrm{Im}B_{k4}$, $|B_{k4}| = [(\mathrm{Re}B_{k4})^2 + (\mathrm{Im}B_{k4})^2]^{1/2}$, $\varphi_{k4} = \frac{1}{4}\arctan\frac{\mathrm{Im}B_{k4}}{\mathrm{Re}B_{k4}}$ [4,7]. Rotation about the z-axis (the four-fold axis) by the angle φ_{k4} eliminates the $\mathrm{Im}B_{k4}$. Then, the new real B_{k4}' is equal to $|B_{k4}|$, and the tetragonal parameters for the remaining k transform correspondingly, whereas the axial CFPs ($q = 0$) remain unchanged. Therefore, the tetragonal II $\mathcal{H}_{\mathrm{CF}}$ for d-electron transition ions can always be parametrized purely by the real CFPs. Similarly, for the hexagonal C_{3h} symmetry the number of CFPs can be reduced from five down to four and is equal to that for D_{3h} symmetry, when the $\mathrm{Im}B_{66}$ is absent due to the higher symmetry [7,8,14]. Such elimination of one of the two $\mathrm{Im}B_{k4}$ CFPs ($k = 4$ or 6) fixes the reference frame, and is equivalent to the lost of one degree of freedom, i.e. the rotation of the reference frame [6]. This fixed frame is imposed on the remaining effective multipoles in the $\mathcal{H}_{\mathrm{CF}}$ to be parametrized.

Let us consider as an example the $\mathcal{H}_{\mathrm{CF}}$ of S_4 point symmetry occurring in paramagnetic ions in the scheelite type crystal structure [7,15]. Then, the complete seven-parameter $\mathcal{H}_{\mathrm{CF}}$ can be written in the form

$$
\begin{aligned}
\mathcal{H}_{\mathrm{CF}}(S_4) = B_{20}C_0^{(2)} \quad &+ \quad B_{40}C_0^{(4)} + |B_{44}|\mathrm{e}^{i4\varphi_{44}}C_4^{(4)} + |B_{44}|\mathrm{e}^{-i4\varphi_{44}}C_{-4}^{(4)} + \\
&+ \quad B_{60}C_0^{(6)} + |B_{64}|\mathrm{e}^{i4\varphi_{64}}C_4^{(6)} + |B_{64}|\mathrm{e}^{-i4\varphi_{64}}C_{-4}^{(6)},
\end{aligned} \tag{19}
$$

where the B_{k4} and B_{k-4} CFPs are only conjugate (Eq.(1)).

This form is usually reduced to the six-parameter one. The B_{4-4} is eliminated rotating the reference frame by the angle φ_{44}, and so we get

$$
\begin{aligned}
\mathcal{H}_{\mathrm{CF}}(S_4) = B_{20}C_0^{(2)} \quad &+ \quad B_{40}C_0^{(4)} + |B_{44}|\left(C_4^{(4)} + C_{-4}^{(4)}\right) + B_{60}C_0^{(6)} + \\
&+ \quad |B_{64}|\mathrm{e}^{i4(\varphi_{64}-\varphi_{44})}C_4^{(6)} + |B_{64}|\mathrm{e}^{-i4(\varphi_{64}-\varphi_{44})}C_{-4}^{(6)}.
\end{aligned} \tag{20}
$$

This formula differs from the real one of the same M in one additional parameter (Eq.(1)) – the phase difference $(\varphi_{64} - \varphi_{44})$ of the complex CFPs, which is an extra parameter in fitting procedures. Now the $max|B'_{60}|$ magnitude for all possible orientations of the reference frame is the maximum of the expression (Eq.(14))

$$
|B'_{60}| = \frac{1}{16}\left|-5 + 105c^2 - 315c^4 + 231c^6 + x_{64}3\sqrt{14}s^4(-1 + 11c^2)\cos 4\left[\alpha - (\varphi_{64} - \varphi_{44})\right]\right| \cdot |B_{60}|, \tag{21}
$$

where $x_{64} = \frac{|B_{64}|}{B_{60}}$. Thus the shift $(\varphi_{64} - \varphi_{44})$ does not change the $max|B'_{60}|$, but influences the relevant distinguished direction compared to that for the real parametrization and, in consequence, modifies the spatial orientation of the considered multipole.

Let us note that in the case of the tetragonal I $\mathcal{H}_{\mathrm{CF}}$, i.e. for real CFPs, there is no such possibility – the orientation of the considered 2^k-pole is absolutely determined by the x_{k4}-ratio. The result is that the complex $\mathcal{H}_{\mathrm{CF}}$ parametrizations enable some extra modifications of the spatial orientation of the component multipoles in fitting procedures when the absolute values of the CFPs are conserved.

5. Discussion

The maximal admissible magnitudes of the B_{k0} CFPs, their variation ranges as well as the relevant distinguished directions depending on the reference frame orientation for all classes of the equivalent parametrizations for the tetragonal including cubic $\mathcal{H}_{\mathrm{CF}}$s have been thoroughly analyzed. The analysis was inspired by observation that in any reference frame the entire magnitudes of M_k cannot be generally achieved by the parameters of the $\mathcal{H}_{\mathrm{CF}}$ 2^k-pole component, particularly by the axial parameters B_{k0} for even $k \geq 2$. The only exception is the purely axial $\mathcal{H}_{\mathrm{CF}}$s for which $\frac{max|B'_{k0}|}{M_k} = 1$ if the reference system z-axis is in line with the symmetry axis. The quadrupole $(k = 2)$ is a special case (not to mention vectors with $k = 1$) since $|B'_{20}|$ can reach M_2 for $x_2 = B_{22}/B_{20} = \frac{\sqrt{6}}{2}$ [16], but this case does not concern the considered symmetries.

The calculated dependencies of the $\frac{max|B'_{k0}|}{M_k}(x_k)$ for $k = 4, 6$ on the $\mathcal{H}_{\mathrm{CF}}$ 2^k-pole composition represented by the appropriate x ratio are shown in Figs 2 and 4. They offer the general review of all particular points of the maps $\frac{B'_{k0}}{M_k}(\alpha, \beta)$ establishing their positions and giving the relevant values for any x_4 and x_6 ratios. The $\frac{max|B'_{k0}|}{M_k}$ values can serve as discriminants of all the equivalent parametrizations which have the same form in the common symmetry adapted system.

The degree of reduction of the $\frac{max|B'_{k0}|}{M_k}$ discriminants with respect to 1 is more tangible for $k = 6$ than for $k = 4$. The whole ranges of the discriminants as functions of x are limited. The lower limits

of $\frac{max|B'_{40}|}{M_4}$ and $\frac{max|B'_{60}|}{M_6}$ amount to 0.7395 and 0.6074, respectively, whereas for comparison in the case of quadrupole $\frac{|B'_{20}|}{M_2} \geq 0.8660$ [16]. The envelopes $\frac{max|B'_{k0}|}{M_k}$ vs. x are characterized by a sharp local minimum at the intersection point of the two plots representing the two various conditions for the extremum, and a weak flat maximum for the ratios $x_{44} = 1.3944$ and $x_{64} = 1.8708$ corresponding to the co-planar square and cubic coordinations, respectively. These particular x ratios can be linked up with the coordination geometry. Taking into account the point symmetry of the central ion surroundings and $1/R$ dependence of the individual ligand potential one gets [4]

$$
\begin{aligned}
\frac{B_{44}}{B_{40}} &= \pm\frac{\sqrt{70}}{2(2\cot^4\theta - 12\cot^2\theta + 3)}, \\
\frac{B_{64}}{B_{60}} &= \pm\frac{3\sqrt{14}}{2}\frac{5\cot^2\theta - 1}{2\cot^6\theta - 30\cot^4\theta + 45\cot^2\theta - 5)},
\end{aligned}
\tag{22}
$$

where θ and R stand for the spherical coordinates of the ligands forming a square. The sign of the ratios depends on the x and y axes orientation with respect to the square.

The distinguished directions corresponding to the maximal magnitudes of $\frac{|B'_{k0}|}{M_k}(x)$ are presented in Fig.8. All the directions are defined with respect to the reference frame in which the initial parametrization is expressed [1,8].

The above investigations provide the distinguished directions for all the component multipoles separately, but they are also obligatory for the resultant $\mathcal{H}_{CF}$. These are the directions that could be used in a possible reduction of the number of independent CFPs [12], as well as examining the standardization of equivalent parametrizations [17,18]. The recognition of the distinguished directions for individual 2^k-poles gives their autonomous spatial orientation and throws light on the mechanism how the component multipoles combine into the resultant effect. The role of the mutual orientation of the component multipoles is clearly noticeable while the real (five-parameter) tetragonal parametrizations of $\mathcal{H}_{CF}$ are compared with the more general complex (seven- or six-parameter) iso-modular parametrizations. The latter is more capable in fitting procedures what implies directly from the possibility of modification of the component multipoles mutual orientation. Dealing with the lower symmetry $\mathcal{H}_{CF}$, in which the component multipoles contain more than one complex-conjugate pairs of CFPs, some intra-multipoles modifications are also possible.

The $\frac{B'_{40}}{M_4}(\alpha, \beta)$ and $\frac{B'_{60}}{M_6}(\alpha, \beta)$ maps for three representative, well-documented parametrizations of the tetragonal $\mathcal{H}_{CFS}$ significantly differing in x_{44} and x_{64} ratios are shown in Figs 5-7 as an example. The maps in Fig.5 show the variation of the B_{40} and B_{60} CFPs depending on the reference frame z-axis direction for the Pr^{3+} ion embedded in the KY_3F_{10} matrix [19]. Its $\mathcal{H}_{CF}$ of C_{4v} point symmetry is characterized by the following parameters (in cm^{-1}): $B_{20} = -589$, $B_{40} = -1711$, $B_{44} = 519$, $B_{60} = 657$, $B_{64} = -196$; $M_2 = 589$, $M_4 = 1862$, $M_6 = 713$; $x_4 = -0.303$, $x_6 = -0.298$.

The maps in Fig.6, in turn, apply to the cubic $\mathcal{H}_{CF}$ with the characteristic ratios $x_4 = 0.5976$, and $x_6 = -1.8708$ [3-5,13]. The system $Pr^{3+}:Cs_2NaRCl_6$ is given here as an example, and, the O_h CF potential is defined by the CFPs (in cm^{-1}): $B_{40} = 2326$, $B_{60} = 247$; $M_4 = 3045$, $M_6 = 699$ [20].

Successively, the maps in Fig.7 refer to the B_{40} and B_{60} CFPs variation for Pr^{+3} ion in Pr_2CuO_4 [21], i.e. in the C_{4v} CF potential of the ratios $x_4 = -0.830$, $x_6 = 9.99$, and the CFPs (in cm^{-1}) are correspondingly equal to: $B_{20} = -294$, $B_{40} = -2302$, $B_{44} = 1910$, $B_{60} = 147$, $B_{64} = 1469$; $M_2 = 294$, $M_4 = 2991$, $M_6 = 1476$. With the exception of the cubic case the remaining x_4 and x_6 ratios come from fittings experimental data.

The particular points marked on the maps (Figs 5–7) by the letters are also noticeable on the diagrams (Figs 2 and 4) as the intersection points of the appropriate diagram branches with the vertical straight lines corresponding to the involved x_4 and x_6 ratios. The intersection points with the highest branches refer to the $\frac{max|B'_{k0}|}{M_k}$ discriminants.

Figs 2 and 4 present the variation of the particular points location on the maps $\frac{B'_{k0}}{M_k}(\alpha, \beta)$ with x_4 and x_6. Since the $\frac{B'_{k0}}{M_k}(\alpha, \beta)$ maps can be considered as the representations of the parent parametrizations, further conclusions concerning the links and genealogy of various CF potentials, their optimal higher-symmetry approximations, etc. may be drawn based on the evolution of such maps while descending in the central ion symmetry, what can be simulated by its shifts inside the coordination polyhedron in various directions. Although the results presented in this paper concern the equivalent $\mathcal{H}_{\mathrm{CF}}$ parametrizations, from the point of view of the maximal axial parameters of component multipoles and their relevant distinguished directions they have more general character going beyond the crystal-field approach.

References

[1] Mulak J and Mulak M 2005 *J. Phys. A: Math. Gen.* **38** 6081

[2] Rudowicz C and Sung H W F 2003 *Physica* **B337** 204

[3] Görller-Walrand C and Binnemans K 1996 *Rationalization of crystal-field parametrization* in: Gschneidner K A Jr and Eyring L (eds) *Handbook on the Physics and Chemistry of Rare Earths*, (Amsterdam: Elsevier) vol.23 pp.121-283

[4] Mulak J and Gajek Z 2000 *The Effective Crystal-Field Potential* (Amsterdam: Elsevier) chap.2

[5] Newman D J and Ng B 2000 in: Newman D J and Ng B (eds) *Crystal Field Handbook* (Cambridge, MA: Cambridge University Press)

[6] Rudowicz C and Qin J 2003 *Phys. Rev. B* **67** 174420

[7] Rudowicz C 1985 *Chemical Physics* **97** 43

[8] Rudowicz C and Qin J 2004 *J. Lumin.* **110** 39

[9] Wybourne B G 1965 *Spectroscopic Properties of Rare Earths* (New York: John Wiley)

[10] Edmonds A R 1960 *Angular Momentum in Quantum Mechanics* (Princeton, NY: Princeton University Press)

[11] Hamermesh M 1989 *Group Theory and Its Application to Physical Problems* (New York: Dover)

[12] Burdick G W and Reid M F 2004 *Molecular Physics* **102** 1141

[13] Hutchings M T 1964 *Sol. State Phys.* **16** 227

[14] Rudowicz C 1986 *Chemical Physics* **102** 437

[15] Mulak J 1993 *Polish J. Chem.* **67** 2053

[16] Mulak J and Mulak M 2006 *J. Phys. A: Math. Gen.* **39** 6919

[17] Rudowicz C and Bramley R 1985 *J. Chem. Phys.* **83** 5192

[18] Rudowicz C 1986 *J. Chem. Phys.* **84** 5045

[19] Morrison C A and Leavitt R P 1982 *Spectroscopic properties of triply ionized lanthanides in transparent host crystals* in: Gschneidner K A Jr and Eyring L (eds) *Handbook of the Physics and Chemistry of Rare Earths*, (Amsterdam: North-Holland) vol.5 p.655

[20] Morrison C A, Leavitt R P and Wortman D E 1980 *J. Chem. Phys.* **73** 2580

[21] Riou G, Jandl S, Poirier M, Nekvasil V, Divis M, Fournier P, Greene R L, Zhigunov D I and Barilo S N 2001 *Eur. Phys. J.* **B23** 179

FIGURE CAPTIONS

FIG.1 The dependence of $\frac{B'_{20}}{|B_{20}|}$ on the reference frame rotation angle β for tetragonal $\mathcal{H}_{\text{CFS}}$ (Eq.4).

FIG.2 $\frac{|B^{(i)}_{40}|}{M_4}$ vs $|x_4|$ plots, where $i = a, b, c, d, e$ denotes one out of the five conditions (Eq.10) or the particular points of the map $\frac{B'_{40}(\alpha,\beta)}{M_4}$, (Eq.11). The vertical straight lines refer to: $|x_4| = 0.303$ for Pr^{3+}:KY_3F_{10} [19]; $|x_4| = 0.598$ for Pr^{3+}:Cs_2NaRCl_6 [20], and $|x_4| = 0.830$ for Pr_2CuO_4 [21], respectively.

FIG.3 $\beta(x_6)$ functions for (e) and (e') conditions (Eq.18); for (f) and (f') conditions the plots are symmetrical with respect to x_6.

FIG.4 $\frac{|B^{(i)}_{60}|}{M_6}$ vs $|x_6|$ plots, where $i = a, b, c, d, e, e', f, f'$ denotes one out of the eight conditions (Eq.17) or the particular points of the map $\frac{B'_{60}(\alpha,\beta)}{M_6}$, (Eq.18). The vertical straight lines refer to: $|x_6| = 0.298$ for Pr^{3+}:KY_3F_{10} [19] and $|x_6| = 1.871$ for Pr^{3+}:Cs_2NaRCl_6 [20]; for Pr_2CuO_4 $x_6 = 9.99$ [21].

FIGS 5a, 5b The maps $\frac{B'_{40}(\alpha,\beta)}{M_4}$ and $\frac{B'_{60}(\alpha,\beta)}{M_6}$ for Pr^{3+}:KY_3F_{10} [19], C_{4v} point symmetry; the initial CFPs (in cm^{-1}) are $B_{40} = -1711$, $B_{60} = 657$; $M_4 = 1862$, $M_6 = 713$; $x_4 = -0.303$, $x_6 = -0.298$; the particular points are marked by the letters.

FIGS 6a, 6b The maps $\frac{B'_{40}(\alpha,\beta)}{M_4}$ and $\frac{B'_{60}(\alpha,\beta)}{M_6}$ for Pr^{3+}:Cs_2NaRCl_6 [20], O_h point symmetry; the initial CFPs (in cm^{-1}) are $B_{40} = 2326$, $B_{60} = 247$; $M_4 = 3045$, $M_6 = 699$; $x_4 = 0.5976$, $x_6 = -1.8708$; the particular points are marked by the letters.

FIGS 7a, 7b The maps $\frac{B'_{40}(\alpha,\beta)}{M_4}$ and $\frac{B'_{60}(\alpha,\beta)}{M_6}$ for Pr^{3+} in Pr_2CuO_4 [21], C_{4v} point symmetry; the initial CFPs (in cm^{-1}) are $B_{40} = -2302$, $B_{60} = 147$; $M_4 = 2991$, $M_6 = 1476$; $x_4 = -0.830$, $x_6 = 9.99$; the particular points are marked by the letters.

FIG.8 The ranges of the distinguished directions characterized by the maximal values of $|B'_{k0}|$ CFPs depending on the $|x|$ ratios for tetragonal $\mathcal{H}_{\text{CF}}$'s ($|x_4| = 0.5976$ and $|x_6| = 1.8708$ are the cubic ratios, the β angle between the distinguished direction and the z-axis is given within the round brackets).
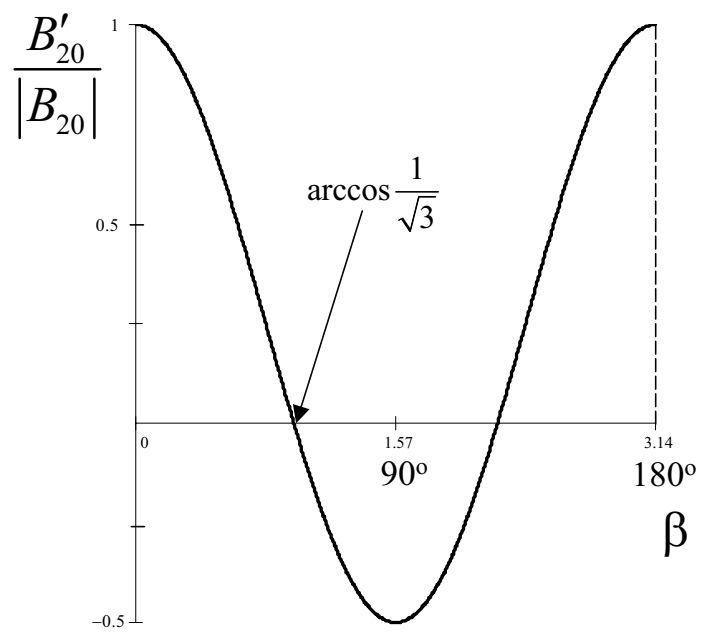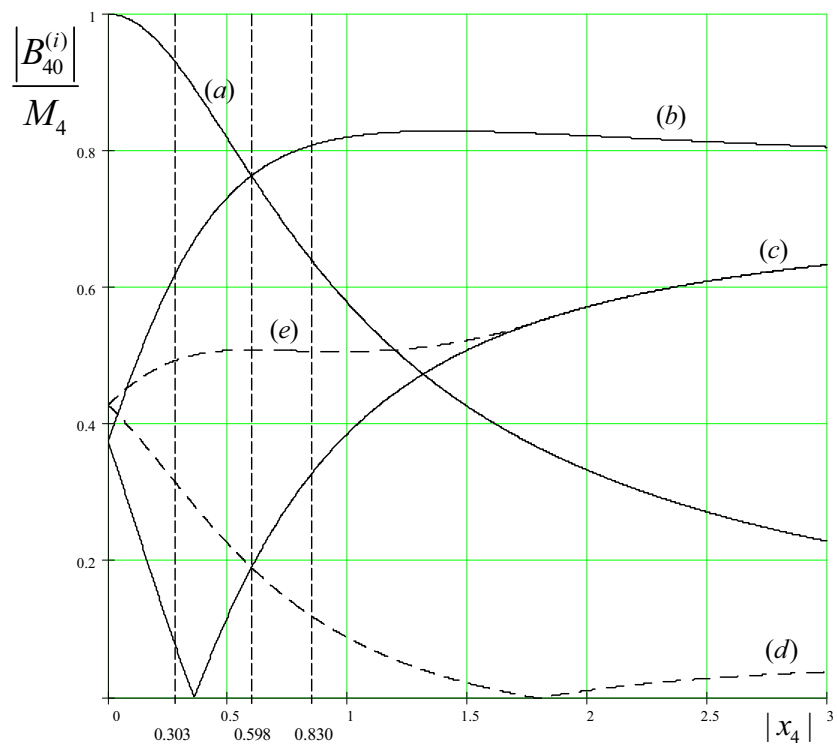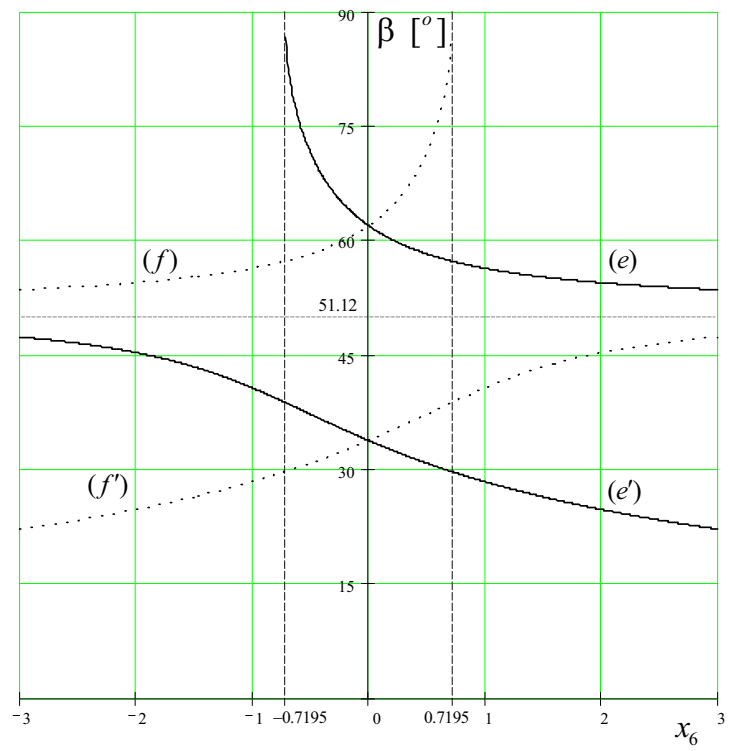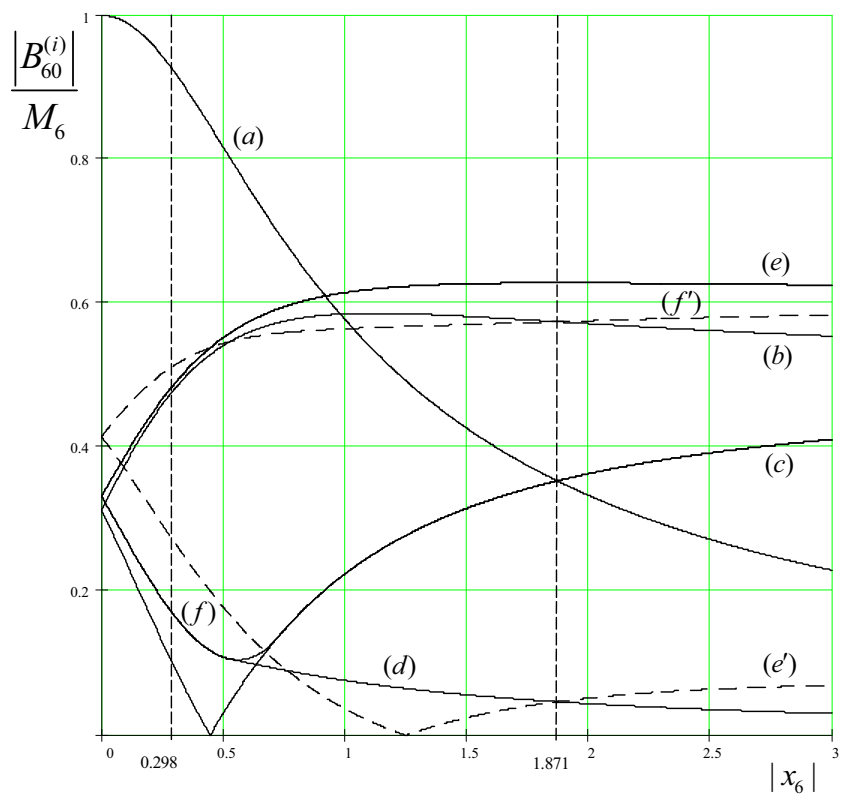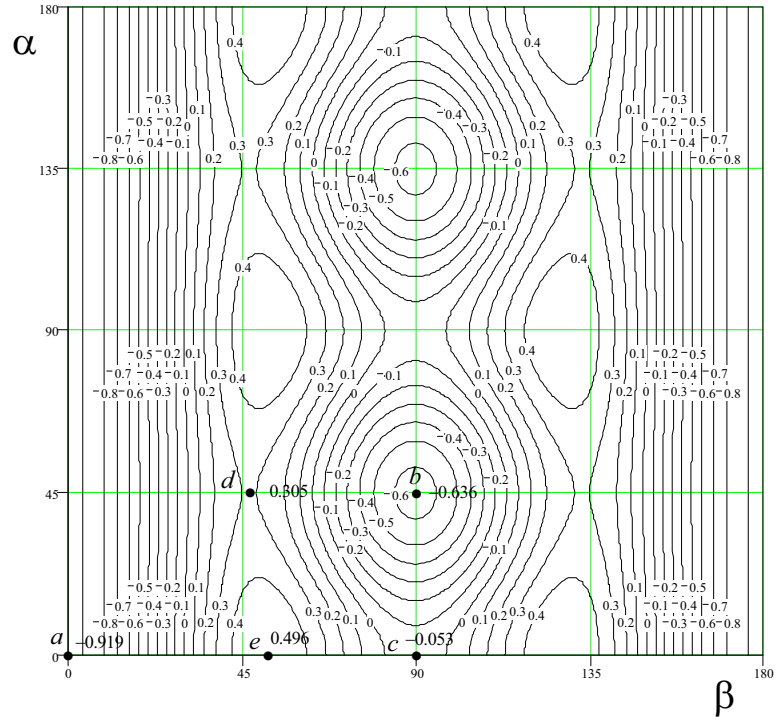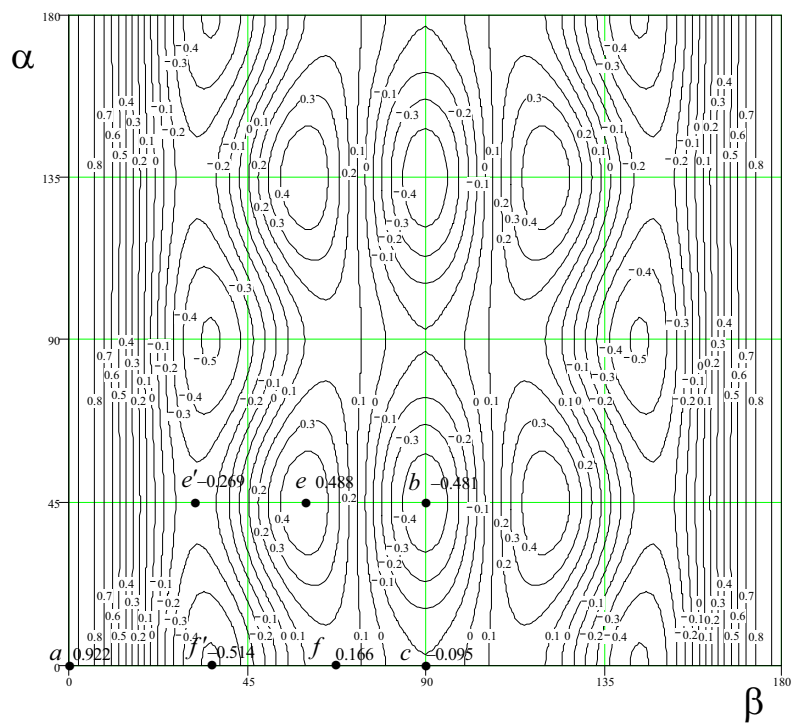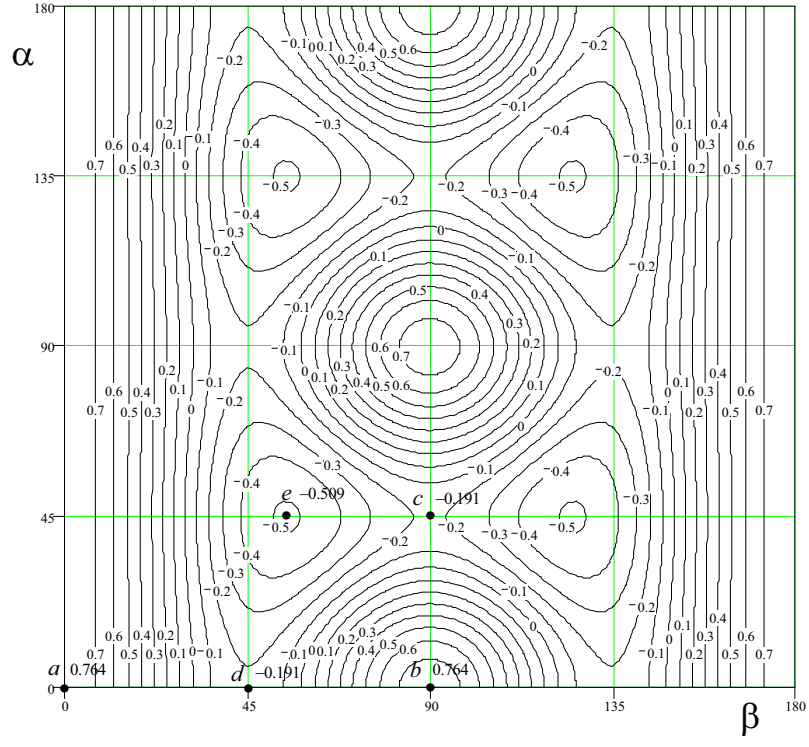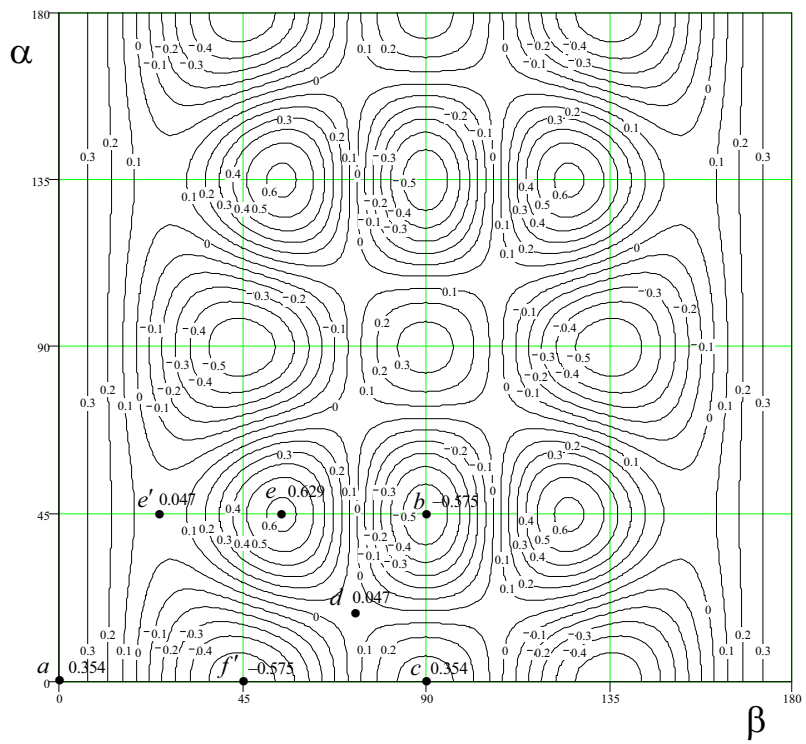
Fig.1.

Fig.2.

Fig.3.

Fig.4

Fig.5a

Fig.5b

Fig.6a

Fig.6b

Fig.7a

Fig.7b

Fig.8.